Deliverable 2.3:
Links Between Land Cover Change and Climate in the Horn of Africa

For the partnership:
Akash Koppa (UGent), Jeroen Claessen (UGent), Abdul Muktadir (UGent), Dave MacLeod (UBristol), Diego G. Miralles (UGent)

Table of Contents

List of Acronyms Used in this Report

COSMO	Consortium for Small-scale Modeling
CLM	Community Land Model
CRU TS	Climate Research Unit gridded Time Series
CSGC	Conditional Spectral Granger Causality
FLEXPART	Flexible Particle Dispersion Model
FVC	Fractional Vegetation Cover
GLEAM	Global Land Evaporation Amsterdam Model
GDHY	Global Dataset of Historical Yield
IGBP	International Geosphere-Biosphere Programme
MODIS	Moderate Resolution Imaging Spectrometer
PDSI	Palmer Drought Severity Index
SEDI	Standard Evapotranspiration Deficit Index
SPEI	Standardized Precipitation and Evapotranspiration Index

1. Introduction

Land cover and land use significantly impact the global and regional water, energy, and biogeochemical cycles (Foley et al., 2005; Alkama and Cescatti, 2015). Accurately quantifying and monitoring long-term land cover changes is thus necessary for reliable assessment of changes in regional climate, water resources, and ecosystem services. Globally, direct anthropogenic activities (such as deforestation and afforestation, expansion of agriculture, and urbanization) and indirect effects (such as climate change) are primary drivers of land cover change (Song et al., 2018). The Horn of Africa is no exception. In the past decades, the region has witnessed increased economic and population growth. To ensure adequate food security, the Horn of Africa experienced agricultural intensification at the expense of natural ecosystems, including farmlands and pastures. In addition, population growth has resulted in a steady replacement of natural vegetation with human settlements and urban centers (Dadi et al., 2016). These land cover disturbances have already impacted the regional hydrological cycle with significant changes seen in both water quantity in the form of streamflow and water quality (Dinka and Klik, 2019).

While land cover change can have direct measurable impacts on the hydrological cycle, its relationship with climate is more complex. Changes in land cover can alter not only the chemical composition of the atmosphere but also directly affect the physical attributes that affect the water and energy exchange with the atmosphere, such as albedo and surface roughness (Feddema et al., 2005). Conversely, the altered atmospheric conditions can influence the land cover through changes in the regional precipitation and aridity (Lian et al., 2021). For example, evidence has been presented that the Gezira large scale irrigation project in East Africa has enhanced regional rainfall (Alter et al., 2015). Further, modeling studies have shown that human-induced changes of forests to cropland and pastures (as those experienced in the Horn of Africa) can increase the frequency of heatwave and drought occurrence (Findell et al., 2017). As droughts and heatwaves can have far-reaching consequences on food security, living conditions, and civil conflicts (Hsiang et al., 2013), it is important to study the linkages between land cover changes and regional climate. Moreover, the impact of such land cover changes in the regional climate of the Horn of Africa have not been systematically studied.

Here, the primary objective is to understand and quantify the links between land cover change and regional climate in the Horn of Africa. To achieve this, we first present a comprehensive analysis of the land cover change using satellite-based datasets over the last two decades (Section 2). Next, we focus on exploring the trends in crop yields in the region and, since most of the agriculture is dependent entirely on rainfall, the links between yield and drought occurrence are investigated (Section 3). In Section 4, we quantify the main climatic drivers of vegetation dynamics, thus providing evidence of the role of climate as a driver of land cover change in the Horn of Africa. Finally, we provide a roadmap for continuing the presented studies and new research which will target closing the other component of the land cover–climate feedback: quantifying the impact of land cover change on the regional climate.

2. Recent Land Cover Changes

To quantify the spatiotemporal changes in land cover across the Horn of Africa, we use two datasets derived from the Moderate Resolution Imaging Spectrometer (MODIS) instrument above the Terra and Aqua satellites from NASA. The first dataset (MCD12Q1) provides 500m spatial resolution discrete land cover classification based on the International Geosphere-Biosphere Programme (IGBP) scheme (Friedl and Sulla-Menashe, 2019) at an annual time step. The second dataset (MOD44B) provides continuous fractional vegetation cover (FVC) information at 250m spatial resolution at an annual timestep (DiMiceli et al., 2015). We analyze the land cover changes over the Horn of Africa for a period of 20 years (2001–2019).

We first analyze the change in land cover by comparing the maps of the most dominant land cover type per pixel between two 5-year periods: 2001–2005 and 2015–2019. A visual inspection of the land cover maps in Figure 1a shows that, during 2001–2005, grasslands were the most widespread land cover type in the Horn of Africa region, covering approximately 48% of the total area, followed by open shrublands (16.5%, concentrated in parts of Somalia and eastern Ethiopia). Figure 1b shows the dominant land cover types for 2015–2019, and highlights that these two land cover types still dominate the Horn of Africa landscape. Both croplands and savannas cover roughly 8% of the region, and are primarily concentrated in the Ethiopian highlands. We see that the land cover follows a strong climatic gradient from the dry northeastern Somalian desert to the more humid Ethiopian highlands, where evergreen needleleaf forests are also present. To better understand the trend in these four dominant land cover types, we construct a yearly time series of the percentage of total area (3.05 million sq. km) occupied by each of them. We note here that the total area estimate includes only the land surface encompassed by the Horn of Africa in Figure 1a. It is evident from Figure 1c that the grasslands have been slowly expanding from 2001 until 2019, with a slight downward trend between 2013–2016 (Dadi et al., 2016). In contrast, the open shrublands exhibit a steady downward trend from the beginning of the study period. The total extension of croplands and savannas does not show significant changes across the satellite record (Figure 1c).

We also performed a per-pixel analysis of land cover change and summarized the results in a Sankey diagram (Figure 2), which quantifies the transformation of a specific land cover type into other land cover types between the two time periods (2001–2005 and 2015–2019). We see that approximately 1.5% of the cropland area in the 2001–2005 time period was transformed into a different land cover type, with the majority being converted into grasslands, and a small percentage into savannas. However, the net loss in croplands is 0.2% of the total land area as other land cover types have been converted to agricultural land (1.3% of the total land area or approx. 40,000 sq. km). Grasslands have witnessed the biggest gross gain in terms of area, with savannas and closed shrublands being the biggest contributors, in addition to croplands. Between the periods of 2001-2005 and 2015-2019, grasslands have increased (net gain) by approx. 36,600 sq. km (1.2% of the total HAD area). It is interesting to note that a considerable

area of evergreen broadleaf forests (0.3% of the total area or approx. 9,100 sq. km of area have been converted into savannas, indicating possible effects of deforestation (Bullock et al., 2021).

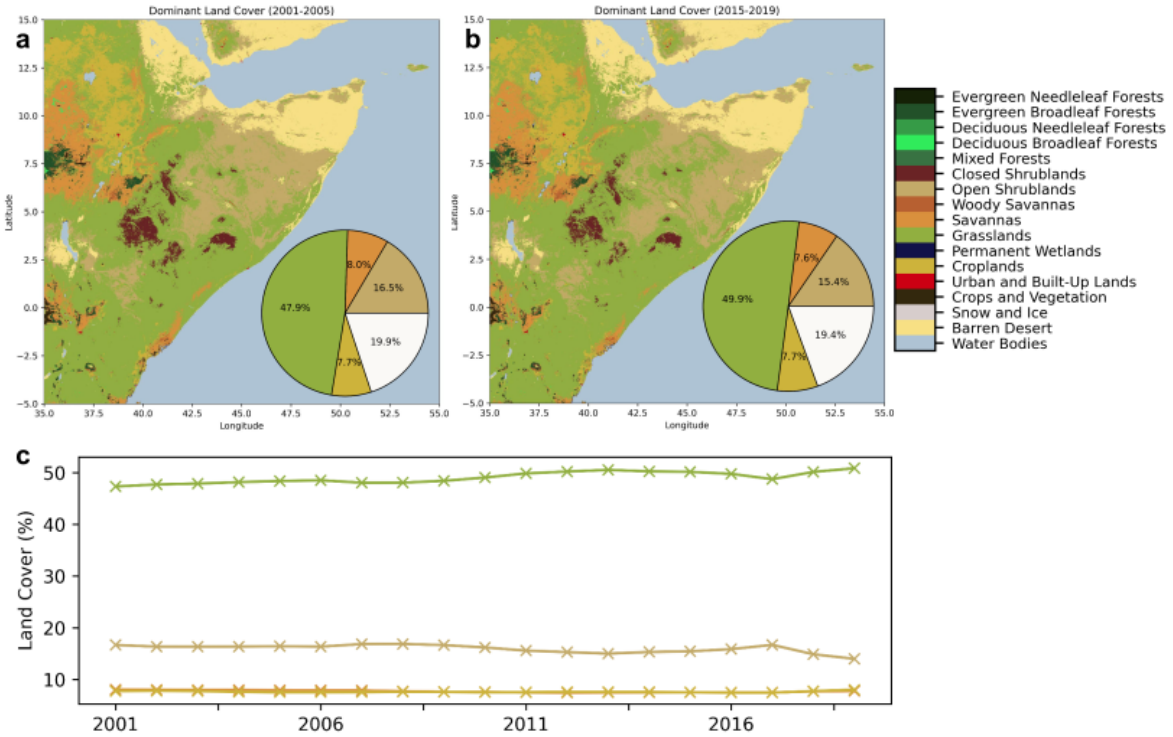

Fig. 1: Maps of dominant land cover per pixel during the five-year periods between (a) 2001–2005 and (b) 2015–2019. The net coverage of the four dominant land cover classes (grasslands, open Shrublands, savannas, and croplands is shown in the pie diagrams; the white color represents the aggregate of all the other land cover classes. (c) Time series of the four major land cover classes over the time span 2001–2019 (expressed in percentage of the total area). The land cover classification is based on the International Geosphere-Biosphere Programme (IGBP) scheme and is sourced from the Moderate Resolution Imaging Spectrometer (MODIS) land cover type dataset (MCD12Q1).

Next, we quantify changes in vegetation cover using a continuous FVC dataset. The value of fractional cover varies from 0 (no vegetation) to 1 (fully covered with vegetation). Figure 3a shows the mean fractional vegetation cover over the Horn of Africa. We see that it follows a climatic and topographic gradient, with densely-covered regions in the Ethiopian and Kenyan Highlands – in the western and southern part of the study region – reaching values >70% vegetation coverage over extensive areas. These regions correspond mostly to grassland, savanna and evergreen broadleaf forest land cover types, as shown in Figure 1. The climatic imprints are also seen in the densely vegetated southern coast, which receives high amounts of rainfall (see Deliverable 2.1). In agreement with Figure 1, the northeast part of the Horn of Africa shows very low vegetation coverage, as expected from the low annual rainfall (Deliverable 2.1). We also quantify the trends in the fractional vegetation cover over a period of 16 years (2001–2016). Some distinct spatial patterns are apparent in the trends map, with reduction in the fractional vegetation cover witnessed in the southeastern parts of the study region. Negative

trends are also found in parts of the Ethiopian highlands, which is in agreement with the reduction in evergreen broadleaf forest extension seen in Figure 1 and Figure 2. Although negative trends in vegetation cover are more widespread, increases in vegetation are seen in the low-lying and arid areas in the north, and also in the forests south of Lake Turkana.

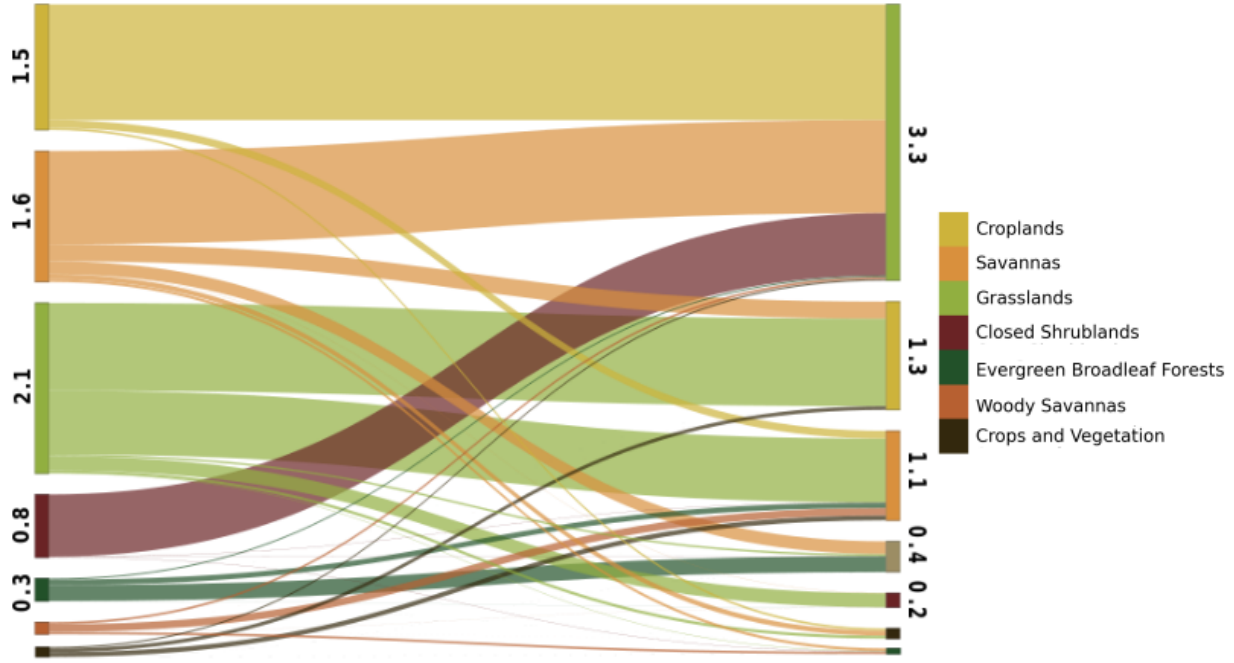

Fig. 2: Sankey Diagram of the land cover change between the periods 2001–2005 and 2015–2019. The diagram shows the percentage of each land cover type that has been converted to a different land cover type between 2001–2005 and 2015–2019. For example, 1.5% of the cropland area has been converted to a different land cover, with the majority being transformed into grasslands. The numbers on the left (right) represent the percentage by which a specific land cover has reduced (increased) between 2001–2005 and 2015–2019.

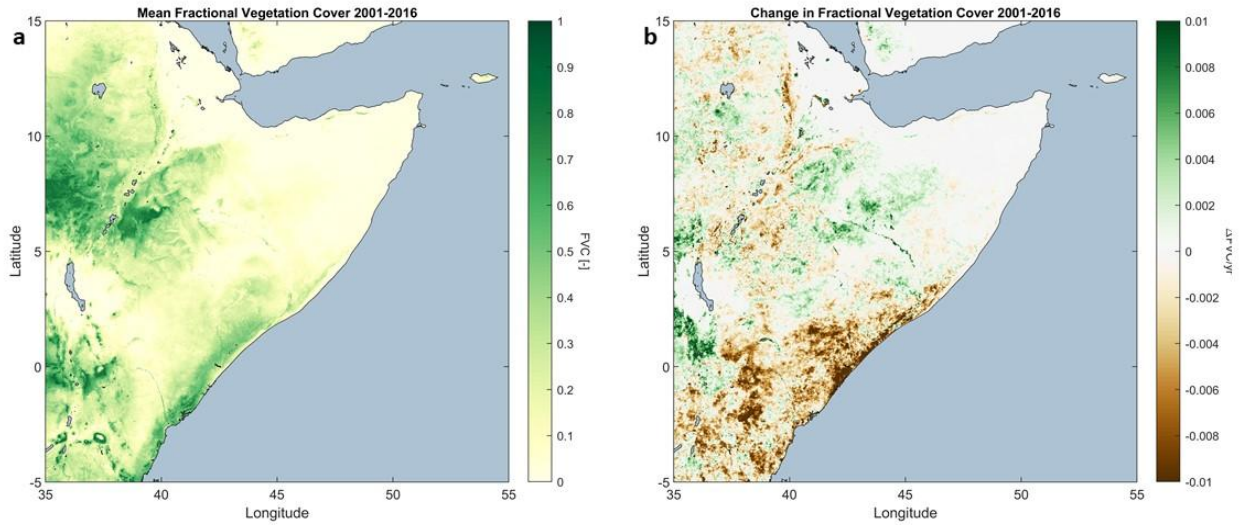

Fig. 3: Changes in vegetation cover and climate drivers over the Horn of Africa for the period 2001–2016. (a) Mean annual fractional vegetation cover. (b) Trends in fractional vegetation cover (ΔFVC/year). FVC data sourced from MODIS: technical details provided in text above.

3. Changes in Crop Yield and Links to Climate

Agriculture and livelihood in the Horn of Africa is especially vulnerable to droughts, since approximately 75% of the workforce is involved in smallholder rainfed agriculture (Salami et al., 2010). For example, the 2010/11 drought in the region affected ten million people and raised mortality tolls by 250,000 people in Somalia (Checchi and Robinson, 2013). Since rainfed agriculture is dominant, it is important to quantify the dependence of agriculture in the Horn of Africa on the variability in regional climate. Specifically, we are interested in the effect of droughts on the yields of the two major crop types in the region: wheat and maize.

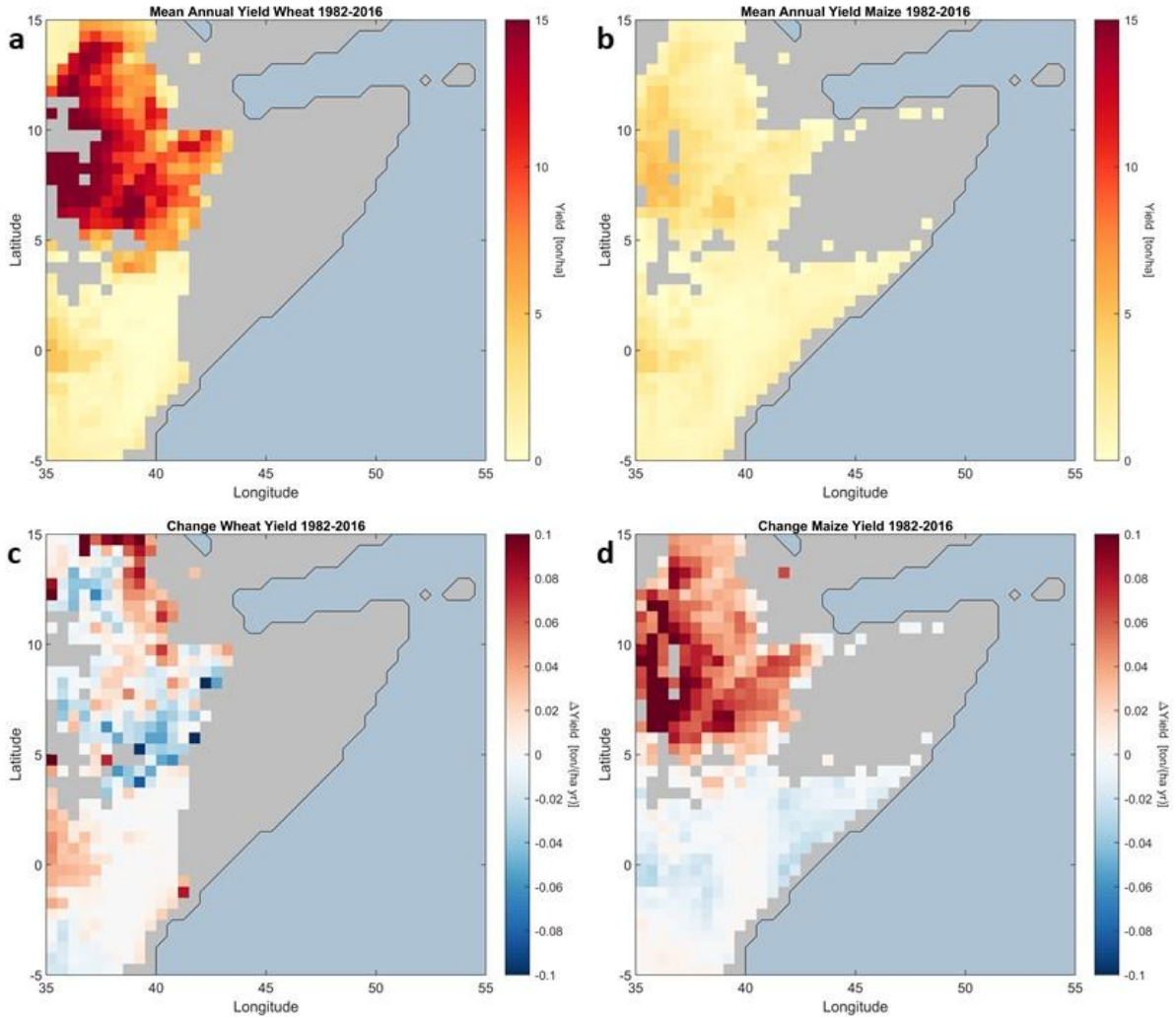

Fig. 4: Yield maps for the Horn of Africa for the period 1982–2016. Mean annual yield [ton/ha] for **(a)** wheat and **(b)** maize. Trends in yield [ton/(ha yr)] for **(c)** wheat and **(d)** maize . Based on the Global Dataset of Historical Yield (GDHY, Iizumi and Sakai, 2020).

Annual gridded data of crop yields (ton/ha) for wheat and maize at a spatial resolution of 0.5° are derived from the Global Dataset of Historical Yield (GDHY, Iizumi and Sakai, 2020) for a period of 25 years (1982–2016). In the region, the growing period of maize is between April and September, and that of wheat is between May and November. The growing season information has been derived from the global crop calendar dataset (Sacks et al. 2010). We note here that the growing and harvesting seasons vary across the Horn of Africa and the selected period encompasses the entire range. For the analysis, only rainfed regions, in which crops depend on rainfall as the major source of water, are considered. The mean annual yield map for wheat (Figure 4a) shows that the major growing regions include large parts of the Ethiopian Highlands (upto 15 ton/ha), and to a lesser extent the Kenyan Highlands in the south (up to 5 ton/ha). In contrast, maize yields are much lower than for wheat (up to 5 ton/ha), with yields per hectare in Ethiopia slightly higher than in Kenya. In terms of trends, wheat yields show strong increases (up to 0.1 ton/ha/year) in the northern and southern parts, but local decreases in wheat yields also occur in parts of Ethiopia (Figure 4c). In contrast the maize yields exhibit a strong geographical gradient with yields increasing in Ethiopia and mildly decreasing in Kenya (Figure 4d).

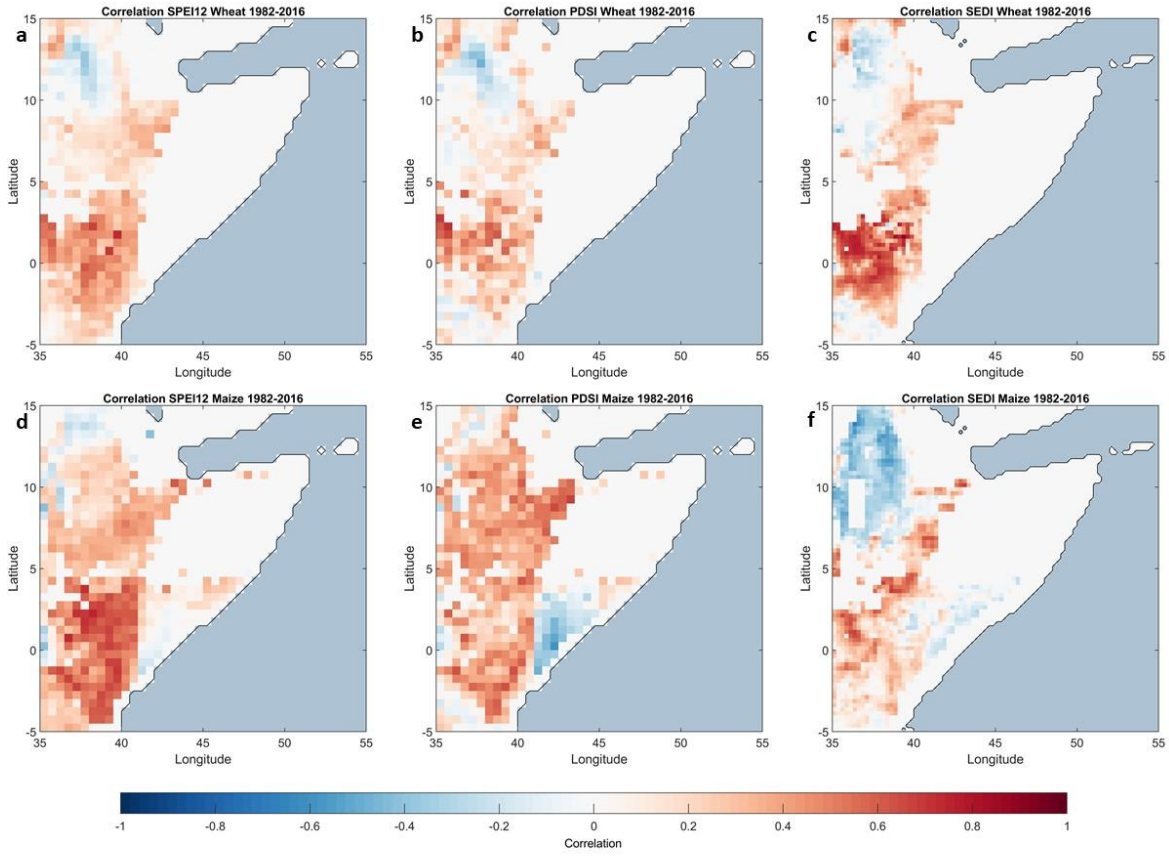

Fig. 5: Correlation maps between crop yield [ton/ha] and drought indices over the Horn of Africa for the period 1982:2016. **(a)** SPEI12 - Wheat **(b)** PDSI - Wheat **(c)** SEDI - Wheat **(d)** SPEI12 - Maize **(e)** PDSI - Maize **(f)** SEDI - Maize. Positive correlation (red) indicates yield loss with drought propagation, whereas negative correlation indicates yield gains.

Next, we quantify the impact of droughts on wheat and maize yields using three widely used drought indices, namely: (a) Standardized Precipitation Evapotranspiration Index (SPEI) (Vicente-Serrano et al., 2010) estimated using the CRU TS version 4.05 (Harris et al., 2020), (b) self-calibrating Palmer Drought Severity Index (PDSI) (Alley, 1984) estimated using the CRU TS 4.05 dataset, and (c) Standard Evapotranspiration Deficit Index (SEDI) (Vicente-Serrano et al., 2018) estimated using the GLEAM dataset (Miralles et al., 2011; Martens et al. 2017). SPEI is a multivariate drought index which considers both precipitation (accounting for water availability) and potential evaporation (to account for the atmospheric evaporative demand). SPEI has been shown to outperform univariate drought indices – such as the Standard Precipitation Index (SPI), which accounts only for the effect of precipitation deficits and thus does not account for the effect of increasing temperatures – in characterizing droughts (Vicente-Serrano et al., 2010). PDSI on the other hand incorporates precipitation, temperature, moisture supply and demand, runoff, and evaporation into a hydrologic accounting system to characterize soil moisture in both wet and drought periods. Finally, SEDI uses the evaporation deficit, i.e, the difference between evaporation and the atmospheric evaporative demand, instead of evaporation and precipitation, to characterize droughts. We note here that we use the SPEI index calculated at a timescale of 12 months (SPEI12), since preliminary analyses showed higher correlations with crop yields for the 12-month aggregation window (not shown).

From Figure 5, it is clear that the correlation of both wheat and maize yields varies across the different drought indices. While SPEI12 and PDSI show strong correlations across the study region, SEDI is negatively correlated with wheat yields in western Ethiopia, a region which receives high precipitation (Figure 5a,b,c). Warmer climate and higher rainfall in this region favors crop growth, consequently yield is usually energy limited (see also Section 4). Hence, the increased temperature associated with drought periods rather helps vegetative growth instead of causing stress, leading to negative correlation. In drier regions, a strong positive correlation is expected as wheat typically shows high sensitivity to heat and water stress. Maize yields show even stronger (negative and positive) correlation with drought indices, although spatial patterns remain similar. SPEI12 and PDSI drought exhibit positive correlation with maize yields across the study region, with Somalia being an exception for PDSI. However, SEDI shows negative correlation in large parts of Ethiopia and Somalia, owing to the energy limited nature of these regions where high rainfall and temperatures favor crop growth, as long as the temperatures are within the optimal plant growth temperature. Additionally, as argued by Abate et al., (2015), negative correlations in Ethiopia may be due to the development and widespread use of a hybrid maize variety which is adapted to local conditions and has increased maize yields even under water limited conditions. Technology-related increases in yield are not considered in drought indices and may also contribute to the negative correlations.

4. Climate Drivers of Vegetation

Changes in vegetation may arise from either anthropogenic disturbances, or past climate variability and natural disturbances such as wildfire, landslides and hurricanes. Anthropogenic disturbances – including deforestation, changes from grasslands to croplands, abandoning

farmlands etc. – sometimes lead to changes in land cover type, as discussed in Section 2. However, vegetation may also respond dynamically to changes in climate, without necessarily implying transitions in land use type. To understand the degree to which climate fluctuations affect vegetation dynamics in the Horn of Africa, we apply a causation inference technique. Conditional Spectral Granger Causality (CSGC) was originally developed in the field of neurology, and it can be used to determine if a variable X causes changes in a target variable Y given any set of additional potential predictors Z_1, Z_2 … Z_n. Instead of determining the generic Granger causality in the time domain – as originally proposed by Granger (1969) and Geweke (1982) – a spectral analogue of Granger causality is applied here, allowing to disentangle causal interactions that are active at different frequencies. A full description of the method can be found in Claessen et al. (2019). We use CSGC to eliminate the influence of low frequency interactions (e.g. seasonal and longer), and concentrate on short-term (e.g. monthly and sub-monthly) interactions between vegetation and climate. Since Granger causality is classically expressed as the ratio of variance measures, we can quantify the variance in vegetation caused by a specific climate predictor.

The mean drivers of vegetation dynamics in the Horn of Africa are shown in Figure 6. The Fractional Vegetation Cover (FVC) is used at the daily timescale as a target variable of the CSGC algorithm, while precipitation, air temperature and solar incoming radiation are used as potential predictors. Using CSGC, we are capable of determining the contribution of each of the three predictors to the FVC independently, while accounting for conditionality between predictors, enabling the interpretation of the results in terms of causation (contrary to traditional correlational analyses).

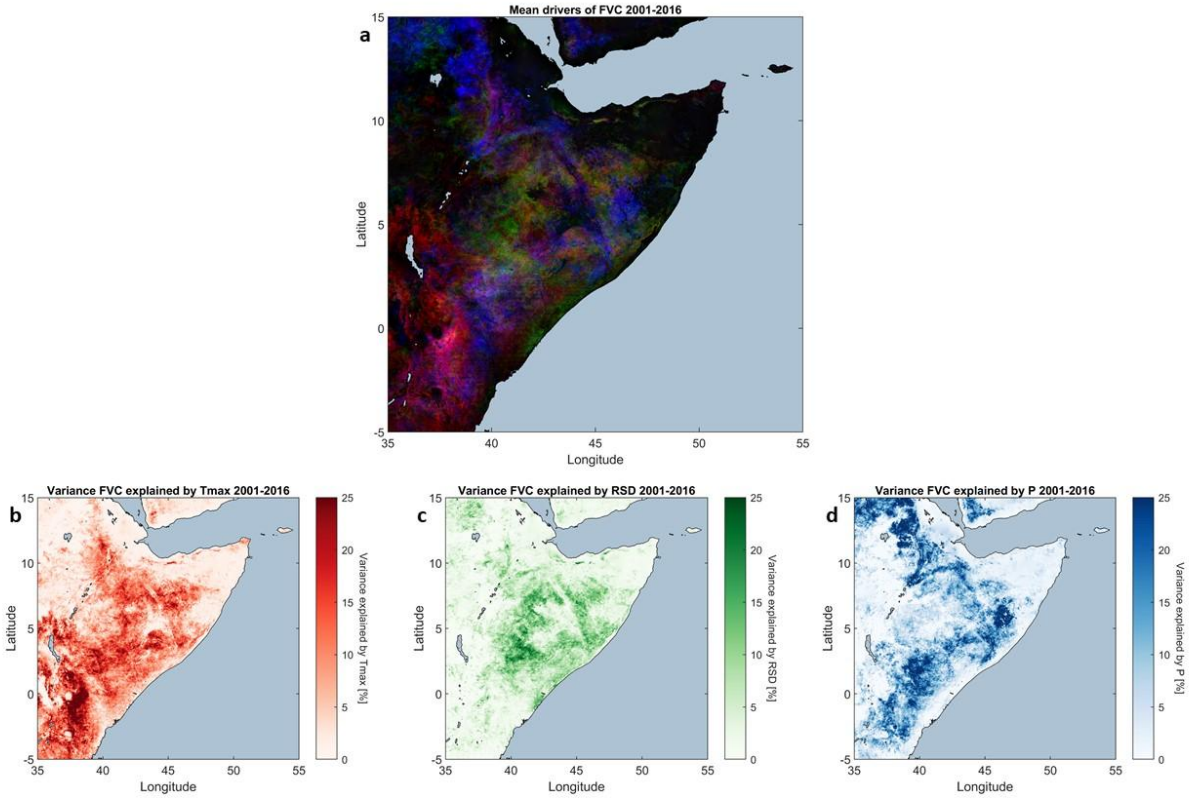

Fig. 6: Variance of vegetation (FVC) explained by temperature, incoming solar radiation and precipitation using CSGC (Claessen et al., 2019) over the Horn of Africa for the period 2001–2016. (a) Trivariate map combining the contributions of the three climatic variables by assigning each predictor to a layer of an RGB image. Black colors indicate no influence by climate on vegetation dynamics, while lighter red implies a dominant influence of temperature (blue: precipitation, green: radiation). (b) Variance explained by maximum temperature, (c) incoming solar radiation, and (d) precipitation. Note that (a) illustrates the sum of the three maps below (b–d). FVC data sourced from the Moderate Resolution Imaging Spectrometer (MODIS) continuous vegetation fraction dataset (MOD44B).

Figure 6 shows a strong spatial heterogeneity with regards to the mean drivers of vegetation over the Horn of Africa. Patterns strongly align with naturally occurring ecosystems (see Section 2) and mean climate patterns (see Deliverable 2.1). Due to the lack of vegetation in desert regions, the influence of climate on land cover dynamics is low. Wetter regions, such as the Ethiopian highlands, are driven by a combination of temperature, radiation and precipitation. Low temperatures may inhibit vegetation growth during specific periods of the year. On the other hand, the arid lowlands of Kenya are strongly forced by temperature, which could point to high temperatures potentially being suboptimal for plant growth. Overall, a transition from water and heat stressed (semi-)arid regimes to relatively more radiation-driven mesic ecosystems is shown in Figure 6. Likewise, the cropland regions shown in Section 3 to be dependent on drought conditions, are identified as primarily water-limited in Figure 6d.

In Figure 6, CSGC is used with the assumption of stationarity, meaning that the interactions of the system are considered to remain constant over time. However, CSGC can be applied to

non-stationary systems. This enables us to address the changing influence of climate drivers of vegetation. Along those lines, Figure 7 shows the trends in the influence of individual climatic factors on vegetation, based on the period from 2001 to 2016.

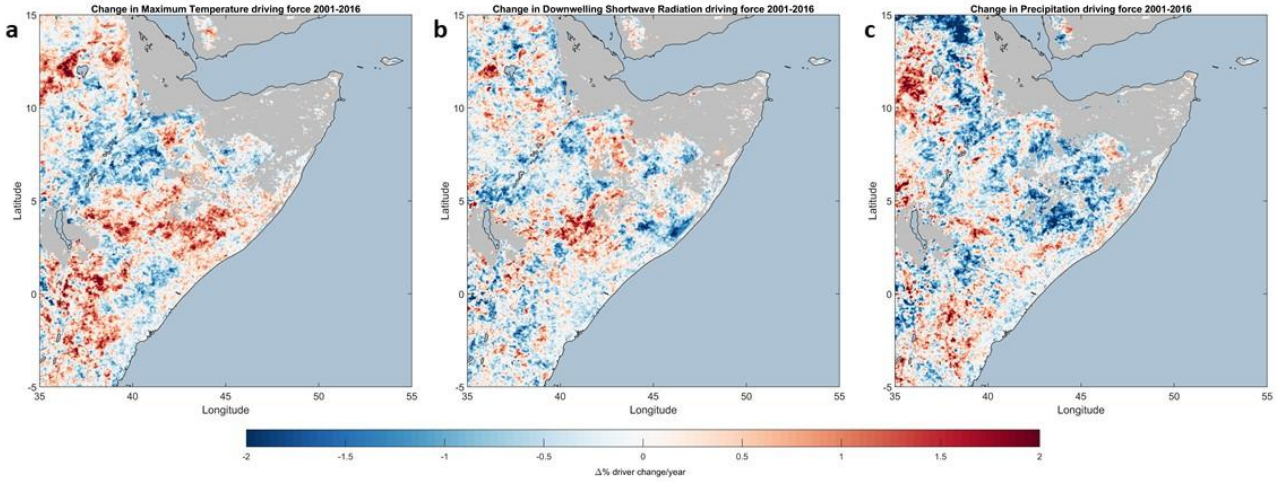

Fig. 7: Trends in the influence of individual climatic factors on vegetation. Trends in the percentage variance of FVC explained by (a) temperature, (b) (b) incoming solar radiation, and (c) precipitation over the Horn of Africa for the period 2001–2016. Blue colors indicate a decrease in the driver, while red points towards an increase of importance. Grey pixels indicate missing data.

While the patterns in Figure 7 are very heterogeneous, an overall increased influence of temperature over vegetation is found over time in the south of the study region – see red colors in Figure 7a. On the other hand, a decreasing influence of precipitation dynamics on vegetation is found over the study period in most semiarid regions; this is indicated by the blue colors in most of Somalia and Ethiopia shown in Figure 7c. A more thorough analysis of these trends, potentially including longer periods, can help identify regions of increased vulnerability to changes in climate. That analysis lies beyond the scope of this report, but will be included in future project activities.

5. Conclusion and Future Work

In this report, we quantified trends in vegetation cover and the land cover change over the Horn of Africa region. The satellite-based datasets used in this study show a steady expansion of grasslands and provide strong evidence of deforestation in the western parts of the region. We also presented observation-based evidence to establish the importance of climate as a driver of changes in both crops and natural vegetation in this region. We found that historically, droughts had a dominant adverse impact on the yields of two major crops in the region, wheat and maize. In addition, the ensemble of drought indices used in the analysis helped identify SPEI12 as the best drought index for monitoring and forecasting yields in the region. Finally, a novel causality

framework was used to map the relative importances of different climatic factors (temperature, precipitation, and radiation) in driving vegetation dynamics at subseasonal timescales across the region, and revealed an enhanced importance of temperature in driving vegetation dynamics in more recent years in the South of the region. Future work involves extending the causality analysis presented here to a time period longer than the one considered here to reliably map regions in which vegetation is vulnerable to changes in climate. Further, research focus will be directed towards unravelling the role of anthropogenic activities on changes in land cover, vegetation, and climate. This will rely on both observation-based causality approaches presented here and new modelling approaches which will combine land regional climate, land surface, and atmospheric transport models. Finally, we will combine the COSMO–CLM, a regional climate and land surface model with the FLEXPART atmospheric transport model to better understand the role of land cover changes on precipitation and temperature patterns in the Horn of Africa region.

References

Abate, T., Shiferaw, B., Menkir, A., Wegary, D., Kebede, Y., Tesfaye, K., Kassie, M., Bogale, G., Tadesse, B., & Keno, T. (2015). Factors that transformed maize productivity in Ethiopia. Food Security, 7(5), 965–981.

Alkama, R., & Cescatti, A. (2016). Biophysical climate impacts of recent changes in global forest cover. Science, 351(6273), 600-604.

Alley, W. M. (1984). The Palmer Drought Severity Index: Limitations and Assumptions. Journal of Climate and Applied Meteorology, 23(7), 1100–1109.

Alter, R. E., Im, E. S., & Eltahir, E. A. (2015). Rainfall consistently enhanced around the Gezira Scheme in East Africa due to irrigation. Nature Geoscience, 8(10), 763-767.

Bullock, E. L., Healey, S. P., Yang, Z., Oduor, P., Gorelick, N., Omondi, S., ... & Cohen, W. B. (2021). Three Decades of Land Cover Change in East Africa. Land, 10(2), 150.

Checchi, F., & Robinson, W. C. (2013). Mortality among populations of southern and central Somalia affected by severe food insecurity and famine during 2010-2012. FAO and FEWSNET, 87 pp. https://www.fsnau.org/in-focus/study-report-mortality-among-populations-southern-and-central-somalia-affected-severe-food-

Claessen, J., Molini, A., Martens, B., Detto, M., Demuzere, M., & Miralles, D. G. (2019). Global biosphere–climate interaction: a causal appraisal of observations and models over multiple temporal scales. Biogeosciences, 16(24), 4851-4874.

Dadi, D., Azadi, H., Senbeta, F., Abebe, K., Taheri, F., & Stellmacher, T. (2016). Urban sprawl and its impacts on land use change in Central Ethiopia. Urban Forestry & Urban Greening, 16, 132-141.

DiMiceli, C., Carroll, M., Sohlberg, R., Kim, D., Kelly, M., Townshend, J. (2015). *MOD44B MODIS/Terra Vegetation Continuous Fields Yearly L3 Global 250m SIN Grid V006* [Data set]. NASA EOSDIS Land Processes DAAC. Accessed from https://doi.org/10.5067/MODIS/MOD44B.006

Dinka, M. O., & Klik, A. (2019). Effect of land use–land cover change on the regimes of surface runoff—the case of Lake Basaka catchment (Ethiopia). Environmental monitoring and assessment, 191(5), 1-13.

Feddema, J. J., Oleson, K. W., Bonan, G. B., Mearns, L. O., Buja, L. E., Meehl, G. A., & Washington, W. M. (2005). The importance of land-cover change in simulating future climates. Science, 310(5754), 1674-1678.

Findell, K. L., Berg, A., Gentine, P., Krasting, J. P., Lintner, B. R., Malyshev, S., ... & Shevliakova, E. (2017). The impact of anthropogenic land use and land cover change on regional climate extremes. Nature communications, 8(1), 1-10.

Foley, J. A., DeFries, R., Asner, G. P., Barford, C., Bonan, G., Carpenter, S. R., ... & Snyder, P. K. (2005). Global consequences of land use. Science, 309(5734), 570-574

Friedl, M., Sulla-Menashe, D. (2019). *MCD12Q1 MODIS/Terra+Aqua Land Cover Type Yearly L3 Global 500m SIN Grid V006* [Data set]. NASA EOSDIS Land Processes DAAC. Accessed from https://doi.org/10.5067/MODIS/MCD12Q1.006

Granger, C. W. J. (1969). Investigating causal relations by econometric models and cross-spectral methods.Econometrica: Journal of the EconometricSociety, pages 424–438

Geweke, J. (1982). Measurement of linear dependence and feedback between multiple time series.Journal of the American Statistical Association,77(378),304–313.

Harris, I., Osborn, T. J., Jones, P., & Lister, D. (2020). Version 4 of the CRU TS monthly high-resolution gridded multivariate climate dataset. *Scientific data*, *7*(1), 1-18.

Hsiang, S. M., Burke, M., & Miguel, E. (2013). Quantifying the influence of climate on human conflict. Science, 341(6151).

Iizumi, T., & Sakai, T. (2020). The global dataset of historical yields for major crops 1981–2016. Scientific data, 7(1), 1-7.

Martens, B., Miralles, D. G., Lievens, H., Van Der Schalie, R., De Jeu, R. A., Fernández-Prieto, D., ... & Verhoest, N. E. (2017). GLEAM v3: Satellite-based land evaporation and root-zone soil moisture. *Geoscientific Model Development*, *10*(5), 1903-1925.

Miralles, D. G., Holmes, T. R. H., De Jeu, R. A. M., Gash, J. H., Meesters, A. G. C. A., & Dolman, A. J. (2011). Global land-surface evaporation estimated from satellite-based observations. *Hydrology and Earth System Sciences*, *15*(2), 453-469.

Lian, X., Piao, S., Chen, A., Huntingford, C., Fu, B., Li, L. Z., ... & Roderick, M. L. (2021). Multifaceted characteristics of dryland aridity changes in a warming world. Nature Reviews Earth & Environment, 2(4), 232-250.

Sacks, W.J., D. Deryng, J.A. Foley, and N. Ramankutty (2010). Crop planting dates: an analysis of global patterns. Global Ecology and Biogeography 19, 607-620. DOI: 10.1111/j.1466-8238.2010.00551.x.

Salami, O., Kamara, A., & Brixiova Schwidrowski, Z. (2010). Smallholder Agriculture in East Africa: Trends, Constraints and Opportunities. African Development Bank Working Papers Series No. 105, African Development Bank, Tunis, Tunisia, 52 pp.

Song, X. P., Hansen, M. C., Stehman, S. V., Potapov, P. V., Tyukavina, A., Vermote, E. F., & Townshend, J. R. (2018). Global land change from 1982 to 2016. Nature, 560(7720), 639-643.

Vicente-Serrano, S. M., Beguería, S., & López-Moreno, J. I. (2010). A Multiscalar Drought Index Sensitive to Global Warming: The Standardized Precipitation Evapotranspiration Index. Journal of Climate, 23(7), 1696–1718.

Vicente-Serrano, S. M., Miralles, D. G., Domínguez-Castro, F., Azorin-Molina, C., El Kenawy, A., McVicar, T. R., ... & Peña-Gallardo, M. (2018). Global assessment of the Standardized Evapotranspiration Deficit Index (SEDI) for drought analysis and monitoring. Journal of Climate, 31(14), 5371-5393.